AIP | Physics of Plasmas

Structure of intermediate shocks in collisionless anisotropic Hall-magnetohydrodynamics plasma models

G. Sánchez-Arriaga

Citation: Phys. Plasmas **20**, 102102 (2013); doi: 10.1063/1.4824001
View online: http://dx.doi.org/10.1063/1.4824001
View Table of Contents: http://pop.aip.org/resource/1/PHPAEN/v20/i10
Published by the AIP Publishing LLC.

Structure of intermediate shocks in collisionless anisotropic Hall-magnetohydrodynamics plasma models

G. Sánchez-Arriaga
Departamento de Física Aplicada, Escuela Técnica Superior de Ingenieros Aeronáuticos, Universidad Politécnica de Madrid, Plaza de Cardenal Cisneros 3, 28040 Madrid, Spain

(Received 18 July 2013; accepted 12 September 2013; published online 1 October 2013)

The existence of discontinuities within the double-adiabatic Hall-magnetohydrodynamics (MHD) model is discussed. These solutions are transitional layers where some of the plasma properties change from one equilibrium state to another. Under the assumption of traveling wave solutions with velocity C and propagation angle θ with respect to the ambient magnetic field, the Hall-MHD model reduces to a dynamical system and the waves are heteroclinic orbits joining two different fixed points. The analysis of the fixed points rules out the existence of rotational discontinuities. Simple considerations about the Hamiltonian nature of the system show that, unlike dissipative models, the intermediate shock waves are organized in branches in parameter space, i.e., they occur if a given relationship between θ and C is satisfied. Electron-polarized (ion-polarized) shock waves exhibit, in addition to a reversal of the magnetic field component tangential to the shock front, a maximum (minimum) of the magnetic field amplitude. The jumps of the magnetic field and the relative specific volume between the downstream and the upstream states as a function of the plasma properties are presented. The organization in parameter space of localized structures including in the model the influence of finite Larmor radius is discussed. © *2013 AIP Publishing LLC*. [http://dx.doi.org/10.1063/1.4824001]

I. INTRODUCTION

Plasma discontinuities are transitional layers where some of the plasma properties change from one equilibrium state to another. A procedure to study these layers consists of constructing *discontinuous solutions* that satisfy the integral form of the equations describing the plasma. For the magnetohydrodynamics (MHD) model, the Rankine-Hugoniot conditions reveal the existence of four types of one-dimensional steady state discontinuities. These are the tangential and contact discontinuities, which do not propagate through the plasma, as well as the shocks and the rotational discontinuities.[1–6] According to their propagation speeds relative to the small-amplitude MHD waves, shock waves are commonly classified as slow, intermediate (IS), and fast. For these waves, the upstream and downstream velocity components normal to the shock and measured in a frame moving with it are, respectively, greater than and less than the slow, the intermediate, and the fast (small-amplitude) wave speeds. All shocks satisfy the coplanarity theorem; but whereas fast and slow shocks do not reverse the magnetic field tangential to the shock front (the rotation angle is $\Delta\phi = 0$), the IS does ($\Delta\phi = \pi$). MHD rotational discontinuities in isotropic plasmas propagate exactly along the normal component of the Alfven speed and rotate the magnetic field component tangential to the shock without changing the thermodynamic state of the plasma.

Discontinuities can also be studied by looking for *continuous solutions* of the system of ordinary differential equations obtained from the fluid model thanks to the stationary traveling wave *ansatz*. This method has been used to find the structure of intermediate shock waves within the resistive-MHD model with[7] and without[8] Hall effect as well as rotational discontinuities in the Hall-MHD model with finite Larmor radius (FLR) effect.[9]

Anisotropic pressure, an effect normally found in space plasmas, has been also considered to extend the analysis of the Rankine-Hugoniot conditions.[10–14] A common problem of anisotropic fluid models is related with the equations of state used to close the system, an historically difficult issue. Some authors avoided it by introducing two parameters that define the plasma anisotropy downstream and upstream.[11,13] However, if one is interested in the structure of the discontinuity, two equations of state to close the system are more convenient. One possibility, adopted in the present work, is the use of the double-adiabatic model,[15] which neglects the parallel heat fluxes considered in numerical simulations by other authors.[16–18] The advantage of this simplification, only valid in limit cases, is to gain insight into the physics of the problem (see for instance Ref. 19). Other pressure assumptions based on observations or even letting the two exponents in the equations of state as free parameters could be also considered in the model. This choice, however, was not followed here because the system has already a large number of free parameters (five). Further, the methodology and some of the main conclusions of this approach does not depend on the equations of state and would not change if these two additional parameters are included. It is also remarkable that the double-adiabatic model is consistent with the derivation of the Hall-MHD system with FLR effect,[20] which was considered in the past to study the structure of rotational discontinuities.[9]

This work discusses the existence of ISs in collisionless plasmas, i.e., transitions from super-Alfvenic to sub-Alfvenic flow that involve the reversing of the magnetic

field transverse to the shock front. Its existence gave rise to controversy in the past. Since the MHD IS wave can only exist for $\Delta\phi = \pi$, it was argued that it constitutes a singular solution and it was rejected as non-physical.[4] Later works using the resistive MHD model showed, however, that IS do exist and are stable.[21–23] Numerical[24–26] and observational[27] evidences of ISs have confirmed them. The collisionless solutions presented here were first obtained in Ref. 28 but the physical significance was unclear for the author. The main difference between the resistive and collisionless intermediate shocks is related with their organization in parameter space; whereas the existence of resistive shocks does not require any relation between the physical parameters, nondissipative structures happen if certain relationship of the shock velocity and its propagation angle with respect to the ambient magnetic field is satisfied. Shocks solutions, which asymptotically tend to different states at infinity, frequently exhibit a constraint that relates two physical parameters. An example is the frequency-velocity relationship exhibited by shocks waves in relativistic plasmas.[29] The appearance in nature of these structures is linked with their stability properties, an issue beyond the scope of the present work.

Thanks to the traveling wave *ansatz*, the double-adiabatic Hall-MHD system leads to a pair of coupled differential equations with a Hamiltonian structure.[28] This property allows the use of some results and tools from dynamical system theory. For instance, the upstream and downstream equilibrium states are fixed points of the system and the ISs are heteroclinic orbits joining them. Homoclinic orbits, which start and end at the same fixed point, are also of great interest because they represent solitary waves. Simple arguments, based on the dimension of the system and its reversibility, help to find the organization of the ISs in parameter space. These results are important because they do not depend on the pressure assumptions and can also be used to obtain information about the existence of solitary waves when FLR effects are included [see Sec. V]. Besides their applications to plasma discontinuities analysis, the computation of heteroclinic orbits and the determination in parameter space of its domain of existence are interesting for other reasons. In first place, since these waves are exact solutions of the fluid model, they can be used to validate numerical codes. Second, as it will be seen, these waves are organized in branches that separate different regimes of bright and dark solitary waves.

The work is organized as follows. Section II briefly summarizes the derivation of the dynamical system that governs the dynamics of the traveling waves and discusses the necessary conditions for the existence of ISs. In Sec. III, the possible upstream and downstream states of the plasma, which correspond to the fixed points of the system, are computed. It also presents the parameter domain where discontinuities are expected to appear. Section IV shows some numerical ISs and the jumps of the magnetic field as a function of the relevant parameters. Finally, the main results and some considerations about the FLR effects are discussed in Sec. V.

II. BASIC EQUATIONS AND CONSIDERATIONS

A. The double-adiabatic Hall-MHD model

The purpose of this work is to present steady state self-consistent ISs solutions of the double-adiabatic Hall-MHD system. This model is only valid to study low-frequency phenomena and it neglects the displacement current and the electron inertia while imposing the quasineutrality approximation. Mass density ρ, plasma flow velocity $\mathbf{v}$, and magnetic field $\mathbf{B}$ are governed by

$$\frac{\partial \rho}{\partial t} + \nabla \cdot (\rho \mathbf{v}) = 0, \tag{1a}$$

$$\frac{\partial}{\partial t}(\rho \mathbf{v}) + \nabla \cdot \left[\rho \mathbf{v}\mathbf{v} + \mathbf{P}_i + \mathbf{P}_e - \frac{1}{4\pi}\left(\mathbf{B}\mathbf{B} - \frac{1}{2}B^2\mathbf{I}\right)\right] = 0, \tag{1b}$$

$$\frac{\partial \mathbf{B}}{\partial t} = \nabla \times \left[\mathbf{v} \times \mathbf{B} - \frac{m_i c}{4\pi e \rho}(\nabla \times \mathbf{B}) \times \mathbf{B}\right]. \tag{1c}$$

The above system is completed by assuming isotropic and anisotropic pressure tensors for electron and ion, respectively,

$$\mathbf{P}_e = p_e \mathbf{I}, \quad \mathbf{P}_i = (p_\parallel - p_\perp)\frac{\mathbf{B}\mathbf{B}}{B^2} + p_\perp \mathbf{I} \tag{2}$$

and isothermal electrons (with temperature T_e) and a double-adiabatic model for the ion pressure

$$p_e = \rho v_{se}^2, \tag{3}$$

$$\frac{p_\parallel}{p_{\parallel 0}} = \left(\frac{B_0}{B}\right)^2 \left(\frac{\rho}{\rho_0}\right)^3 \equiv P_\parallel, \tag{4}$$

$$\frac{p_\perp}{p_{\perp 0}} = \frac{B}{B_0}\frac{\rho}{\rho_0} \equiv P_\perp. \tag{5}$$

Here, $p_{\parallel 0}$ and $p_{\perp 0}$ are the parallel and perpendicular ion pressure components at upstream (or downstream) and $v_{se} = \sqrt{kT_e/m_i}$.

The analysis is restricted to one-dimensional $(\partial/\partial y = \partial/\partial z = 0)$ traveling wave solutions with all quantities depending on $X = x - Ct$ and satisfying the boundary conditions

$$\rho \to \rho_0, \quad \mathbf{v} \to 0, \quad \mathbf{B} \to \mathbf{B}_0(\cos\theta \mathbf{i} + \sin\theta \mathbf{k}) \tag{6}$$

as $X \to +\infty$ or $X \to -\infty$. With these assumptions, Eq. (1a) gives the plasma velocity component along the propagation direction

$$\frac{v_x}{C} = 1 - \frac{\rho_0}{\rho} \equiv 1 - u \tag{7}$$

with u the relative specific volume. Defining the normalized magnetic field $b_{y,z} = B_{y,z}/B_0 \sin\theta$, the longitudinal component of Eq. (1b) gives

$$F(u, b^2) \equiv u - 1 + \frac{1}{2}M_A \sin^2\theta (b^2 - 1) + P = 0 \tag{8}$$

with $b^2 = b_y^2 + b_z^2$,

$$P \equiv M_e\left(\frac{1}{u} - 1\right) + M_i\left[P_\perp - 1 + (a_{p0}P_\parallel - P_\perp)\frac{\cos^2\theta}{\hat{b}^2} - (a_{p0} - 1)\cos^2\theta\right], \tag{9}$$

$\hat{b}^2 = \cos^2\theta + b^2\sin^2\theta, a_{p0} \equiv p_{\parallel 0}/p_{\perp 0}, M_A \equiv V_A^2/C^2, M_e \equiv v_{se}^2/C^2$ and $M_i \equiv v_\perp^2/C^2\,(v_\perp^2 \equiv p_{\perp 0}/\rho_0)$. Therefore, u is a function of just b^2, $u = u(b^2)$. It can be shown that Eq. (8) can be solved only in an interval $b_{min}^2 < b^2 < b_{max}^2$ containing $b^2 = 1$.[28] An orbit in the b_y–b_z phase space cannot cross the inner and outer sonic circles defined by the values b_{min}^2 and b_{max}^2. As shown in Ref. 28, the outer sonic circle always exists, whereas the inner sonic circle appears only in certain parameter domain.

The transverse components of Eq. (1b) allows to write v_y and v_z as explicit functions of b_y, b_z, and u

$$\frac{v_y}{C} = \frac{\sin\theta}{\cos\theta}[\chi(u, b^2) - u]b_y, \tag{10}$$

$$\frac{v_z}{C} = \frac{\sin\theta}{\cos\theta}\{[\chi(u, b^2) - u]b_z - [\chi(1, 1) - 1]\}, \tag{11}$$

where

$$\chi(u, b^2) \equiv u - M_A\cos^2\theta + M_i(a_{p0}P_\parallel - P_\perp)\frac{\cos^2\theta}{\hat{b}^2}. \tag{12}$$

The transverse components of Eq. (1c) give[28]

$$\frac{db_y}{d\zeta} = \chi(u, b^2)b_z - \chi(1, 1), \tag{13}$$

$$\frac{db_z}{d\zeta} = -\chi(u, b^2)b_y, \tag{14}$$

where the dimensionless variable ζ is related with X by

$$\frac{dX}{d\zeta} = \frac{V_A^2\cos\theta}{\Omega_i C}u. \tag{15}$$

Here, $V_A = B_0/\sqrt{4\pi\rho_0}$ is the Alfven velocity and $\Omega_i = eB_0/cm_i$ is the ion-cyclotron frequency. The system (13) and (14), which must be solved self-consistently with Eq. (8), depends on the following 5 parameters: θ, a_{p0}, M_A, M_e, and M_i. For convenience, Refs. 28 and 30 will be followed and some of the results will be given as a function of C/V_A instead of M_A.

System (13) and (14) has two properties with important consequences in the computation of shocks and solitary waves. First, the system is reversible because solutions are invariant under the transformation $(\zeta, b_y, b_z) \to (-\zeta, -b_y, b_z)$. Second, since the model has no irreversible effects, it has a Hamiltonian structure with Hamiltonian

$$H(b_y, b_z) = \frac{1}{2}\int_1^{b^2}\chi(u(a), a)da - \chi(1, 1)(b_z - 1). \tag{16}$$

This function is conserved along the orbits because it does not dependent explicitly on ζ.

B. Considerations about the dynamical system

The derivation of the dynamical system (13) and (14) from the fluid model requires setting boundary conditions as $\zeta \to +\infty$ or $\zeta \to -\infty$. This plasma state appears in the system as the fixed point $Q_0 \equiv (b_y, b_z) = (0, 1)$ $(u = 1)$, which has zero Hamiltonian value. Solutions connecting the fixed point Q_0 with itself (other fixed point) are called homoclinic (heteroclinic) orbits and they represent solitary (shock) waves.

The organization of homoclinic and heteroclinic orbits in parameter space can be discussed taking into account simple geometrical arguments involving the dimensions of the system and the stable and unstable manifolds of Q_0. It should be recalled that the stable (unstable) manifold of a fixed point Q_i is the set of forward (backward) in ζ trajectories that terminate at Q_i. Homoclinic orbits, which connect with Q_0 as $\zeta \to +\infty$ and $\zeta \to -\infty$, must lie in the intersection of both manifolds. For a 2-dimensional system, like system (13) and (14), homoclinic orbits only exist if Q_0 is a saddle (stable and unstable manifolds have dimension equal to one). In this case, both manifolds generically intersect and the homoclinic orbits have codimension zero (the intersection is robust under variation of the parameters). However, the saddle condition is necessary but not sufficient to have homoclinic orbits because it could happen that the orbit hits one of the two sonic circles and Eq. (8) cannot be solved to find $u = u(b^2)$.

Heteroclinic orbits, which connect Q_0 with other fixed point (say Q_1), lie at the intersection of the stable manifold of one fixed point with the unstable manifold of the other. Therefore, a necessary condition is Q_0 and Q_1 to be saddles. In addition to this, since the Hamiltonian is conserved along the orbits, the connection is only possible if both fixed points have the same value of H. This condition only happens for certain combination of the parameters, making the existence of heteroclinic orbits a codimension-one problem. For instance, for M_e, M_i, and a_{p0} fixed, shock waves appear in branches $\theta = \theta(M_A)$ in the $M_A - \theta$ plane (or $C/V_A - \theta$).

In summary, the existence of ISs requires: (i) another fixed point different to Q_0, say Q_1, (ii) both Q_0 and Q_1 must be saddles, (iii) the Hamiltonian at Q_1 should vanish, and (iv) the orbit joining both fixed points cannot hits the outer or the inner sonic circle. As we will see, the simultaneous occurrence of all these conditions does only happen in certain parameter domain that must be computed numerically in general.

Condition (ii) for the fixed point Q_0 was studied in Ref. 28. The sonic velocity (C_s), the firehose velocity (V_F), and the slow (C_{slow}) and fast (C_{fast}) magnetosonic velocities, which can be explicitly written in term of the parameters of the system, define the parameter domain where Q_0 is a saddle. Ordering these four velocities as $C_1 < C_2 < C_3 < C_4$, Q_0 is a saddle if C satisfies $C_1 < C < C_2$ or $C_3 < C < C_4$. Figure (5) in Ref. 28 shows some examples of the stability domains of Q_0 in the $C/V_A - \theta$ plane.

III. FIXED-POINT ANALYSIS AT THE UPSTREAM AND DOWNSTREAM STATES

Simple arguments indicate the absence of shocks in system (13) and (14) with magnetic field rotation different to 0 or π; since Q_0 has magnetic field components $(b_y,b_z)=(0,1)$, such a discontinuity would need the existence of a second fixed point with $b_y \neq 0$, say Q_1. According to Eq. (14), Q_1 would have $\chi(u_1, b_1^2) = 0$ and then Eq. (13) reveals that it would only be possible for parameters satisfying $\chi(1,1) = 0$. One can easily check that, if $\chi(1,1) = 0$, system (13) and (14) conserves b^2 and the locus of the points with $b^2 = 1$ are all fixed points. Therefore, a heteroclinic orbit connecting Q_0 is impossible. As shown in Ref. 9, if the influence of FLR is added in system (13) and (14), rotational discontinuities with magnetic field rotation different to 0 and π are possible.

Once the existence of orbits connecting Q_0 and a fixed point with $b_y \neq 0$ has been ruled out, we pay attention to fixed points with $b_y = 0$. These fixed points satisfy $F(u, b_z^2) = 0$ and $\chi(u, b_z^2)b_z - \chi(1,1) = 0$ [see Eqs. (8) and (13)]. The solutions of this pair of nonlinear algebraic equations have been investigated using the program AUTO,[31] which allows the tracking of the fixed points as a parameter is varied.

Panels (a)–(d) in Fig. 1, which all have parameter values $a_{p0} = 1$ and $M_e = M_i = 0.65M_A$, show the b_z component of several fixed points versus the angle θ for $C/V_A = 0.25$, 0.7, 1.025, and 1.25, respectively. In addition to Q_0, which corresponds to the solid line with $b_z = 1$, the system has other branches of solutions with several turning points (denoted by T_i in Fig. 1). For instance, at $C/V_A = 0.25$, there are five turning points and a θ-range with six fix points. At $C/V_A = 0.7$ [see panel (b)], the turning points denoted by T_1 and T_5 merge and one finds four fixed points for low θ values. At higher velocities, the turning points T_2 and T_3 also merge and disappear, as can be seen in panel (c). For even higher velocity values, the turning point T_4 moves to the left until it reaches $\theta = 0$ and the system has only two fixed points [see panel (d)].

AUTO also computes two-parameter curves of special points like the turning points shown in Fig. 1. This type of diagram allows to delimit in a $\theta - C/V_A$ plane the domains with different number of fixed points. Panels (a)–(d) in Fig. 2 show the results of this calculation for parameter values $a_{p0} = 1$, $M_e = M_i$, and $M_i/M_A = 0.15$, 0.4, 0.65, and 0.9, respectively. The numbers indicate how many fixed points can be found at each parameter domain. For instance, panel (c) in Fig. 2 can be understood by looking at panels (a)–(d) in Fig. 1. At velocity values below $C/V_A \approx 0.62$ and increasing θ, one finds θ-ranges with four, two, four, six, and four fixed points. This feature can also be seen in panel (a) of Fig. 1. For C/V_A above 0.62, the turning points denoted by T_1 and T_5 have merged and the θ-range with just two fixed points disappear (such a merging is reflected in panel (c) of Fig. 2 by a turning point in the $\theta - C/V_A$ plane).

Conditions (ii) and (iii) introduced in Sec. II B are now explored; a heteroclinic orbit is only possible if both fixed points share the Hamiltonian value and they are saddle points. In Figs. 3 and 4, the white (grey) regions are the parameter domains where Q_0 is a saddle (center). The branches $C_I/V_A = C_I/V_A(\theta)$ correspond to parameter combinations with a fixed point (different to Q_0) of zero Hamiltonian value; we used blue solid lines if the fixed point is a saddle and red shaded lines if it is a center. Therefore, solid blue branches within a white domain satisfy conditions (i) to (iii). For convenience, we will call C_I to the velocity of these branches. Depending on the parameters [see panels (a)–(d) in Figs. 3 and 4], we find between two to four branches where the fixed point share the Hamiltonian value with Q_0 but only for one of them the fixed point is a saddle (there is only one blue solid line for each panel). Even though the great variety of fixed points found (up to six in Fig. 2), we now see that the number of shock waves is limited. Further, for fixed values of a_{p0} and the ratios M_e/M_i and M_i/M_A, the branches where shocks waves are possible do not necessarily extend in the whole θ-range $[0, \pi/2]$; as shown for instance in panel (a) of Fig. 3 or Figs. 4(a) and 4(b), the fixed point stability behavior can change from a saddle to a center as θ is decreased. For all panels in Figs. 3 and 4, the velocity C_I

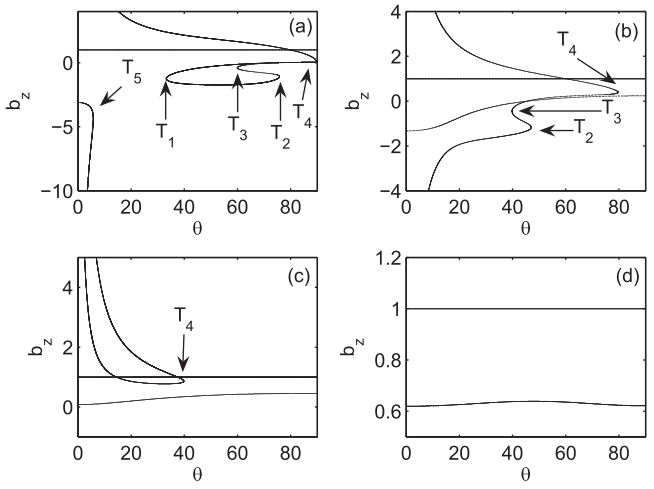

FIG. 1. Fixed points for $M_e = M_i = 0.65M_A, a_{p0} = 1$. Panels (a), (b), (c), and (d) correspond to velocities $C/V_A = 0.25$, 0.7, 1.025, and 1.25, respectively.

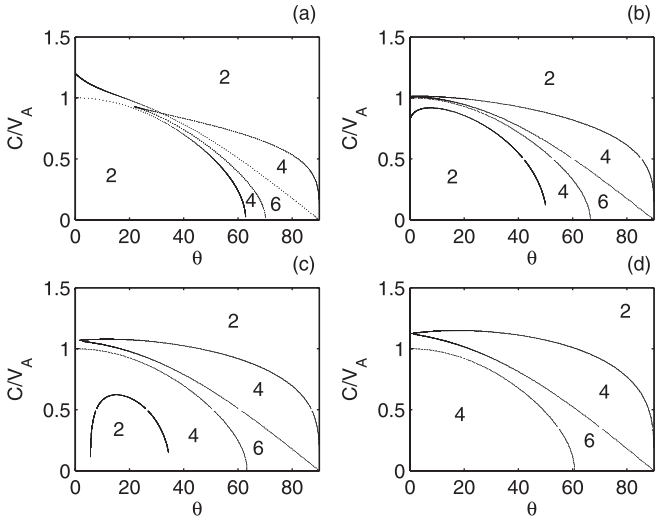

FIG. 2. Number of fixed points in the $\theta - C/V_A$ plane for $a_{p0} = 1$ and $M_e = M_i$. Panels (a), (b), (c), and (d) correspond to $M_i/M_A = 0.15$, 0.4, 0.65, and 0.9, respectively.

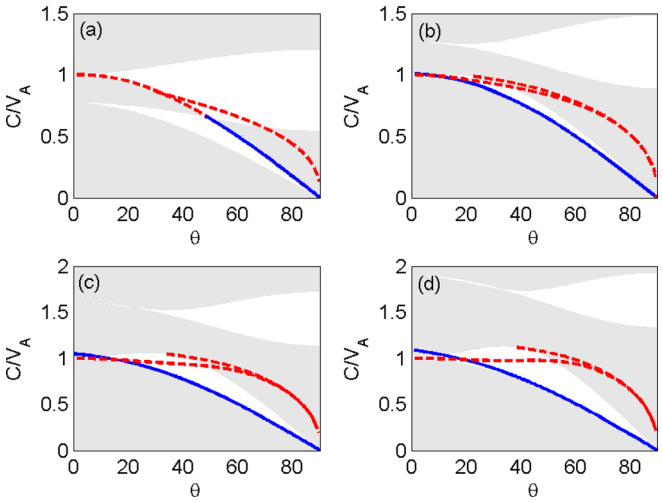

FIG. 3. Branches C_I/V_A versus θ where a fixed point different to Q_0 have $H=0$. Solid blue lines indicate a saddle fixed point and dashed red line a center. Shaded regions correspond to parameter domains where Q_0 is a center. Parameters are $a_{p0}=1$, $M_i=M_e$. Panels (a), (b), (c), and (d) correspond to $M_i/M_A=0.15$, 0.4, 0.65, and 0.9, respectively.

always satisfies $V_F < C_I < C_{slow}$, except in panel (a) of Fig. 3 where $C_{slow} < C_I < V_F$. As panel (a) in Fig. 3 shows, it can exist a fixed point (different to Q_0), which has zero Hamiltonian value and velocity between C_s and C_{fast}. However, it is not possible to construct a discontinuity wave because such a fixed point is a center.

IV. INTERMEDIATE SHOCK WAVES

Discontinuities can exist for parameter values given by the solid blue branches $C_I/V_A = C_I/V_A(\theta)$ lying within a white domain in Figs. 3 and 4. They can be computed by integrating system (13) and (14) with an initial condition along the unstable manifolds of Q_0 or the one belonging to the other connected fixed point, say Q_1. Numerically, this can be done by starting at the initial condition

$$Q_i + \epsilon \mathbf{v}, \tag{17}$$

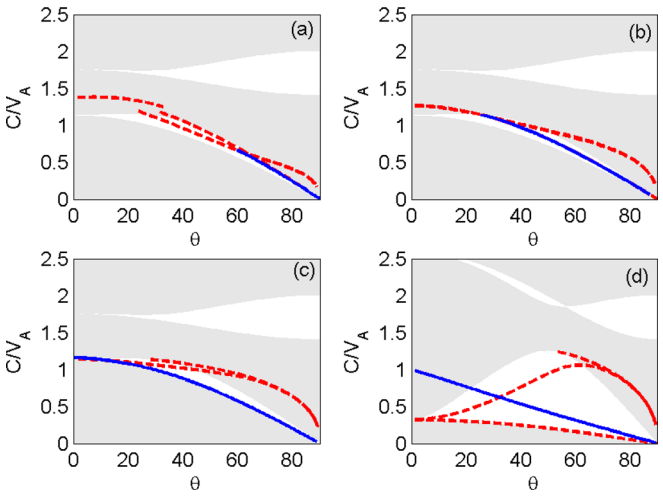

FIG. 4. Similar to Fig. 3 but parameter values $M_i=M_e=M_A$. Panels (a), (b), (c), and (d) correspond to $a_{p0}=0.1$, 0.4, 0.7, and 1.9, respectively.

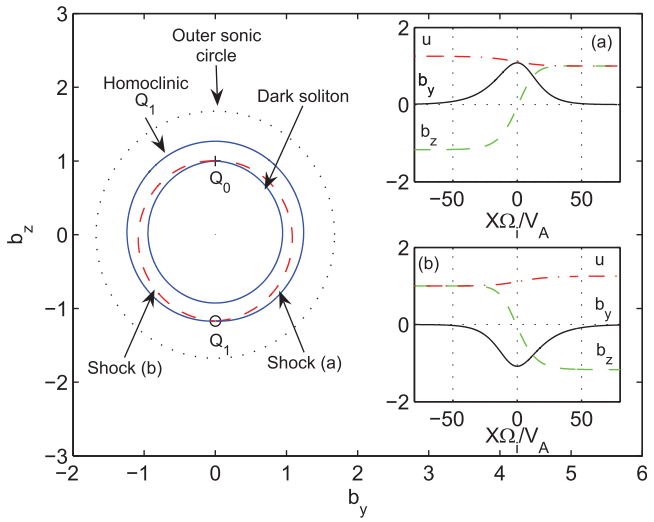

FIG. 5. b_y–b_z phase space diagram for parameter values $M_i=M_e$, $M_i/M_A=0.65$, $a_{p0}=1$, $\theta=80°$, and $C_I/V_A=0.173$. The fix points (cross and circle), the outer sonic circle (black line), the two intermediate shock waves (red dashed lines), the dark soliton (blue line connecting Q_0), and the homoclinic orbit on Q_1 (blue line) are shown. Inset (a) and (b) show the spatial profiles of the shock waves.

where $\mathbf{v}$ is the eigenvector with positive real part of the Jacobian of system (13) and (14) evaluated at the fixed point Q_i ($i=0$ or 1) and ϵ is a small parameter ($\epsilon \approx 10^{-4}$ in our calculations). The result of the integration is a heteroclinic orbit that connects the fixed points Q_0 and Q_1.

Figure 5 shows the b_y-b_z phase space for parameter values $M_i=M_e$, $M_i/M_A=0.65$ and $\theta=80°$. The ratio C/V_A is 0.173 [see panel (c) in Fig. 3]. For clarity, we plotted the outer inner circle (black line) and the fixed points Q_0 (cross) and Q_1 (circle). Two heteroclinic orbits [labeled (a) and (b)] connecting Q_0 and Q_1 can be seen (dashed red lines). To complete the picture, we also plotted the homoclinic orbit on Q_0 (blue solid line), which is a dark solitary wave, and the homoclinic orbit on Q_1. The structure of these solutions (b_y, b_z, and u) versus the dimensionless spatial variable $X\Omega_i/V_A$ are shown in the two insets. The discontinuity with label (a) is electron-polarized and its field amplitude $|\mathbf{B}|$ displays a maximum whereas (b) is ion-polarized and has a minimum (in resemblance with the bright and the dark solitons). Figure 6 displays another example with parameter values $M_i=M_e=M_A$, $\theta=50°$ and $a_{p0}=1.9$ [$C/M_A=0.415$ as shown in panel (d) of Fig. 4]. In this case, there is no homoclinic orbit on Q_1 because it hits the sonic circle.

Insets (a) and (b) in Figs. 5 and 6 illustrate the physical meaning of the heteroclinic connection: it is a continuous transition from one homogeneous plasma state to another where the tangential magnetic field is reversed. They are exact solutions of the double-adiabatic Hall-MHD model involving jumps in the b_z components of the magnetic field and the relative specific volumes u ($u \equiv \rho_0/\rho$). These properties and the value of C_I/V_A allow to classify these solutions as IS waves. The width d of the layer depends on the specific value of the parameters; for instance, d is of the order of tens of V_A/Ω_i in Fig. 5 and a few V_A/Ω_i in Fig. 6. Although the variables describing the shocks are symmetric or antisymmetric with respect the variable ζ, they exhibit an asymmetry

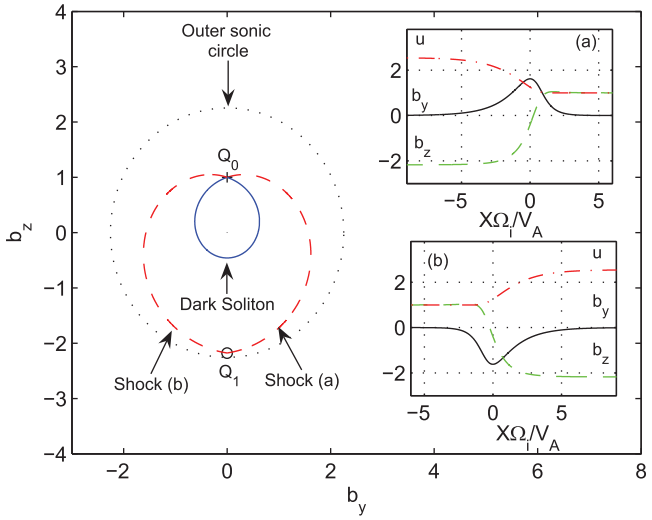

FIG. 6. Similar to Fig. 5 but parameter values $M_i/M_e, M_i/M_A = 1$, $a_{p0} = 1.9$, $\theta = 50°$, and $C_I/V_A = 0.415$. The homoclinic orbit on Q_1 (not shown) hits the outer sonic circle.

behavior with respect to the physical spatial variable X. This is a consequence of Eq. (15), which contains the variable u in the righthand side.

Since Q_0 has $(b_y,b_z) = (0,1)$ and $u = 1$, the magnitude of the jumps along the shocks is controlled by the fixed point Q_1. Panels (a) and (b) in Figs. 7 and 8 show the b_z and u values of the fixed point Q_1 corresponding to the blue solid lines in Figs. 3 and 4, respectively. The value of b_z at Q_1 is always negative, indicating a reversal of the magnetic field and the IS nature of the solutions. Depending on the parameter, the jump along the shock wave of the b_z component can be very large if the angle θ between the direction of propagation of the wave and the ambient magnetic field is small.

The localization in parameter space of the shock waves gives also information about the dark and bright solitary waves. The blue solid lines in Figs. 3 and 4, where shock waves happen, split the $\theta - C/V_A$ plane in two regions where the solitons have different polarization. To illustrate this feature, Fig. 9 shows the dark and bright solitary waves for

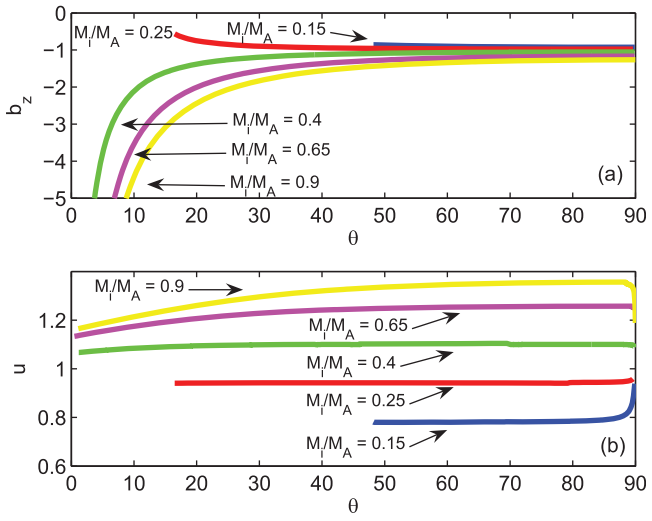

FIG. 7. Values of b_z [panel (a)] and u [panel (b)] at fixed point Q_1 versus θ. Parameter values are $M_i = M_e$, $a_{p0} = 1$, and $C/V_A = C_I(\theta)/V_A$ (see Fig. 3).

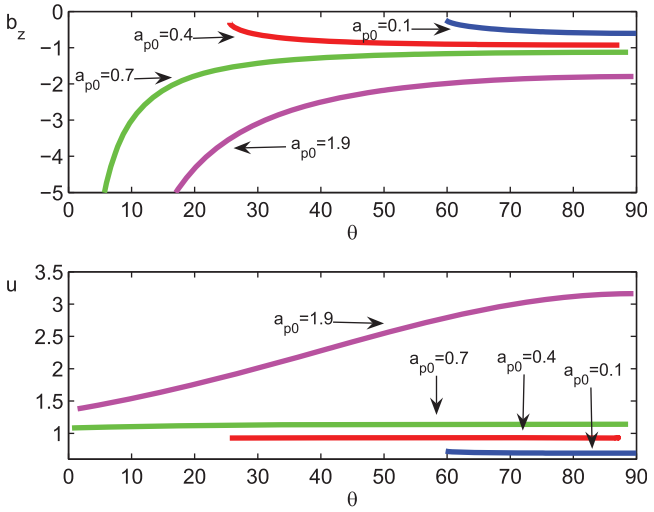

FIG. 8. Values of b_z [panel (a)] and u [panel (b)] at fixed point Q_1 versus θ. Parameter values are $M_i = M_e = M_A$ and $C/V_A = C_I(\theta)/V_A$ (see Fig. 4).

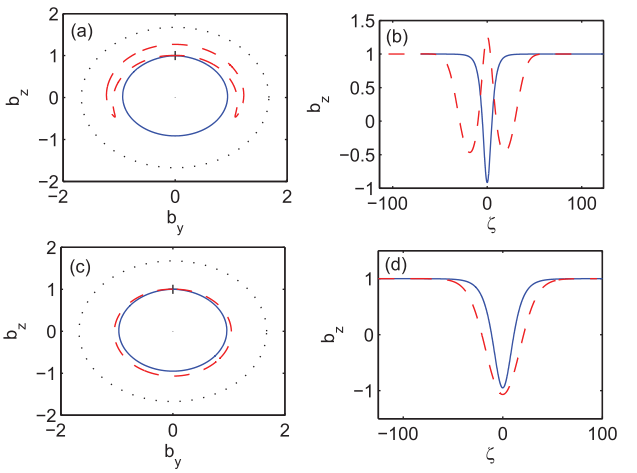

FIG. 9. Solitary waves with parameter values $M_e = M_i$, $a_{p0} = 1$, $M_i = 0.65M_A$, and $\theta = 80°$. Panels (a) and (b) correspond to $C/V_A = 0.1731$ whereas (c) and (d) have $C/V_A = 0.1728$. The bright (dashed red) and the dark (blue solid) solitons are shown. In panels (a) and (c), the fixed point Q_0 (cross) and the sonic circles (dashed black) are also displayed.

parameter values $M_e = M_i$, $a_{p0} = 1$, $M_i = 0.65M_A$, $\theta = 80°$. In panels (a) and (b), the velocity value $C/V_A = 0.1742$ is slightly above the value corresponding to the IS ($C_I/V_A = 0.1740$); whereas in panels (c) and (d), we have $C/V_A = 0.1738$ (between the velocity of the IS and the slow magnetosonic velocity $C_{slow} = 0.1736$). For velocities values above the one corresponding to the IS, the bright soliton has a *banana*-like polarization with a maximum of b_z at the center of the soliton [see panel (b)]. However, for velocities between the slow magnetosonic and the shock velocity, the b_z component of the bright soliton exhibits a minimum [panel (d)].

V. CONCLUSIONS

This work discusses the existence of discontinuities in the double-adiabatic Hall-MHD model. Simple geometrical arguments, based on the dimension of the stable and unstable manifolds of the fixed points, the dimension of the system,

and its reversibility, reveal that discontinuities are organized in branches within the $C/V_A - \theta$ parameter space, i.e., they have codimension equal to one. Bright and dark solitons, however, are robust under parameter variations and have codimension equal to zero. Also, an analysis of the existence of fixed points allowed to ruled out the presence of rotational discontinuities, which present a magnetic field rotation $\Delta\phi$ different to 0 or π. However, such a solution exists if FLR effects are incorporated.[9] All the numerical solutions have $\Delta\phi = \pi$, corresponding with IS waves. We emphasize that a rich variety of fixed points have been found but for most of them continuous solutions cannot be constructed because either they have not vanishing Hamiltonian value or they are centers. The addition of a dissipative term, for instance, the resistivity effect already considered in Refs. 7 and 8, would break the Hamiltonian structure and would make possible shocks solutions with an enhancement of the entropy across the discontinuity.

A deep numerical survey varying all the parameters (except the ratio $M_e/M_i = 1$) was carried out. For fixed values of the ratios M_e/M_i, M_i/M_A, and a_{p0}, a branch of ISs, $C_I/V_A = C_I/V_A(\theta)$, was found for velocities values between the firehose and the slow magnetosonic velocities. Note that the firehose velocity reduces to the shear Alfven or intermediate velocity in the case of isotropic pressure. It seems that the branch always occurs when the IS wave propagates perpendicular to the ambient magnetic field ($\theta \approx 90^\circ$). However, depending on the specific parameter values, it could cease to exist as θ is decreased. Figure 3 reveals that the velocity of the wave is close to the firehose velocity when the anisotropy parameter a_{p0} is equal to one. In Fig. 3, the IS branch practically overlaps with V_F but there is still some room in between where dark and bright solitary waves exist. The distance between V_F and C_I increases with a_{p0} [see panel (d) in Fig. 4]. As shown in Figs. 7 and 8, the IS wave introduce jumps for the b_z magnetic field component and the relative specific volume u. The value of the jump depends on the parameters and can be very large in the case of b_z when $\theta \to 0$ (parallel propagation). Electron polarized ISs display a $|\mathbf{B}|$ maximum and ion-polarized a minimum.

Unless certain relationship between the propagation angle θ and the shock velocity is satisfied, the present model rules out the existence of time-stationary IS. For initial conditions violating this relationship, one may expect time-dependent IS. The evolution of these shocks to time-stationary structures depends on the stability of our solutions, an aspect beyond the scope of the present work. Recent numerical calculations reinforce the ubiquity of intermediate shocks and they highlight their easy excitation;[32,33] simulations of the randomly driven Cohen-Kulsrud-Burger equation show the formation of a large number of structures with a quasi-discontinuity of the phase and without an appreciable variation of their amplitude. These structures, which approximate rotational discontinuities, evolve to intermediate shocks with phase jumps close to π (see Fig. 1 in Ref. 33).

As shown in Ref. 30, the addition of finite Larmor radius is rather challenging because it prevent an explicit relation between the magnetic field and the normal velocity plasma components (Eqs. (10) and (11)). From the point of view of the dynamical system, this extension is very important because it raises the dimension from two to four and the geometrical argument presented in Sec. II B must be reconsidered. It is unknown whether or not a Hamiltonian function would exist in this case, but the system is still reversible. This last issue is very important because the organization in parameter space of the solitary waves (homoclinic orbits) can be done by following Ref. 34. The fixed point Q_0 can be a center, saddle-center, saddle, or focus-focus and the existence of connecting orbits is determined by the dimension of its stable and unstable manifolds. In principle one would expect: (i) no solutions if Q_0 is a center, (ii) branches of solutions if Q_0 is a saddle-center (codimension-one), and (iii) a continuum of solutions if Q_0 is a saddle or a focus-focus (codimension-zero). For parameters making Q_0 a saddle-center, several isolated branches of homoclinic orbits could appear (each of them with a different number of humps). If Q_0 is a focus-focus, a theorem[35] shows that the existence of one transverse symmetric homoclinic orbit implies the existence of infinitely many others. These homoclinic orbits are like multiple copies of the primary orbit separated by finitely many oscillations close to Q_0. The existence of asymmetric orbits must be considered as well. Therefore, the addition of FLR effects (even if small) dramatically change the character of the system and the persistence of solutions computed without finite Larmor terms cannot be guaranteed. A numerical survey keeping in mind the organization in parameter space here introduced would be required to explore the different possibilities.

ACKNOWLEDGMENTS

The author would like to thank Dr. C. Bombardelli for the help in revising the grammar and correct style of the text. This work was supported by the Ministerio de Ciencia e Innovación of Spain (Grant No. ENE2011-28489).

[1]P. Germain, "Shock waves and shock-wave structure in magneto-fluid dynamics," Rev. Mod. Phys. **32**, 951 (1960).
[2]J. E. Anderson, *Magnetohydrodynamic Shock Waves* (1963).
[3]A. Jeffrey and T. Taniuti, *Non-Linear Wave Propagation* (1964).
[4]A. R. Kantrowitz and H. E. Petschek, *MHD Characteristic and Shock Waves* (McGraw-Hill, 1966).
[5]A. I. Akhiezer, I. A. Akhiezer, R. V. Polovin, A. G. Sitenko, and K. N. Stepanov, "Plasma electrodynamics," *Linear Theory*, International Series on Natural Philosophy Vol. 1 (Oxford Pergamon Press, 1975), p. 1.
[6]J. P. Goedbloed, "Time reversal duality of magnetohydrodynamic shocks," Phys. Plasmas **15**(6), 062101 (2008).
[7]L.-N. Hau and B. U. O. Sonnerup, "The structure of resistive-dispersive intermediate shocks," J. Geophys. Res. **95**, 18791, doi:10.1029/JA095iA11p18791 (1990).
[8]L.-N. Hau and B. U. O. Sonnerup, "On the structure of resistive MHD intermediate shocks," J. Geophys. Res. **94**, 6539, doi:10.1029/JA094iA06p06539 (1989).
[9]L.-N. Hau and B. U. O. Sonnerup, "Self-consistent gyroviscous fluid model of rotational discontinuities," J. Geophys. Res. **96**, 15767, doi:10.1029/91JA00983 (1991).
[10]Y. M. Lynn, "Discontinuities in an anisotropic plasma," Phys. Fluids **10**, 2278 (1967).
[11]J. K. Chao, "Interplanetary collisionless shock waves," Rep. CSR TR-70-3, Massachusetts Institute of Technology, Center for Space Research, Cambridge, Massachusetts, 1970.

[12]P. D. Hudson, "Discontinuities in an anisotropic plasma and their identification in the solar wind," Planet. Space Sci. **18**, 1611 (1970).
[13]P. D. Hudson, "Rotational discontinuities in an anisotropic plasma," Planet. Space Sci. **19**, 1693 (1971).
[14]P. D. Hudson, "Shocks in an anisotropic plasma," J. Plasma Phys. **17**, 419 (1977).
[15]L.-N. Hau, T.-D. Phan, B. U. O. Sonnerup, and G. Paschmann, "Double-polytropic closure in the magentosheath," Geophys. Res. Lett. **20**, 2255, doi:10.1029/93GL02491 (1993).
[16]C. L. Tsai, R. H. Tsai, B. H. Wu, and L. C. Lee, "Structure of slow shocks in a magnetized plasma with heat conduction," Phys. Plasmas **9**, 1185 (2002).
[17]C. L. Tsai, B. H. Wu, and L. C. Lee, "Structure of intermediate shocks and slow shocks in a magnetized plasma with heat conduction," Phys. Plasmas **12**(8), 082501 (2005).
[18]C. L. Tsai, H. H. Chen, B. H. Wu, and L. C. Lee, "Structure of fast shocks in the presence of heat conduction," Phys. Plasmas **14**(12),122903 (2007).
[19]D. W. Walthour, J. T. Gosling, B. U. O. Sonnerup, and C. T. Russell, "Observation of anomalous slow-mode shock and reconnection layer in the dayside magnetospause," J. Geophys. Res. **99**, 23705, doi:10.1029/94JA01767 (1994).
[20]A. MacMahon, "Finite gyro-radius corrections to the hydromagnetic equations for a Vlasov plasma," Phys. Fluids **8**, 1840 (1965).
[21]C. C. Wu, "On MHD intermediate shocks," J. Geophys. Lett. **14**, 668 (1987).
[22]C. C. Wu, "The MHD intermediate shock interaction with an intermediate wave—Are intermediate shocks physical?," J. Geophys. Res. **93**, 987, doi:10.1029/JA093iA02p00987 (1988).
[23]C. C. Wu, "Formation, structure, and stability of MHD intermediate shocks," J. Geophys. Res. **95**, 8149, doi:10.1029/JA095iA06p08149 (1990).
[24]C. C. Wu and T. Hada, "Formation of intermediate shocks in both two-fluid and hybrid models," J. Geophys. Res. **96**, 3769, doi:10.1029/90JA02463 (1991).
[25]H. Karimabadi and N. Omidi, "Hybrid simulations of intermediate shocks—Coplanar and noncoplanar solutions," J. Geophys. Res. Lett. **19**, 1723 (1992).
[26]H. Karimabadi, "Physics of intermediate shocks: A review," Adv. Space Res. **15**, 507 (1995).
[27]J. K. Chao, L. H. Lyu, B. H. Wu, A. J. Lazarus, T. S. Chang, and R. P. Lepping, "Observations of an intermediate shock in interplanetary space," J. Geophys. Res. **98**, 17443, doi:10.1029/93JA01609 (1993).
[28]E. Mjølhus, "Velocity amplitude relationships and polarizations in families of MHD solitary waves," Phys. Scr. **T122**, 135 (2006).
[29]D. Farina and S. V. Bulanov, "Dynamics of relativistic solitons," Plasma Phys. Controlled Fusion **47**, A73 (2005).
[30]E. Mjølhus, "Finite Larmor radius influence on MHD solitary waves," Nonlinear Process. Geophys. **16**, 251 (2009).
[31]E. J. Doedel, A. R. Champneys, T. F. Fairgrieve, Y. A. Kuznetsov, B. Sandstede, and X. Wang, *Auto 97: Continuation and Bifurcation Software for Ordinary Differential Equations (with Homcont)* (1997).
[32]D. Laveder, T. Passot, and P. L. Sulem, "Phase slips and dissipation of Alfvenic intermediate shocks and solitons," Phys. Plasmas **19**(9), 092116 (2012).
[33]D. Laveder, T. Passot, and P. L. Sulem, "Intermittent dissipation and lack of universality in one-dimensional Alfvénic turbulence," Phys. Lett. A **377**, 1535 (2013).
[34]A. R. Champneys, "Homoclinic orbits in reversible systems and their applications in mechanics, fluids and optics," Physica D: Nonlinear Phenom. **112**, 158 (1998).
[35]R. L. Devaney, "Homoclinic orbits in Hamiltonian systems," J. Differ. Equations **21**, 431 (1976).